

Fast-Grown Interpenetrating Network in Poly(3-hexylthiophene): Methanofullerenes Solar Cells Processed with Additive

Hsiang-Yu Chen,[†] Hoichang Yang,[‡] Guanwen Yang,[†] Srinivas Sista,[†] Ruben Zadoyan,[§] Gang Li,^{||} and Yang Yang^{*,†}

Department of Materials Science and Engineering, University of California—Los Angeles, Los Angeles, California 90095, Department of Advanced Fiber Engineering, Inha University, Yonghyun-dong 253, Incheon 402-751, Korea, Technology and Applications Center, Newport Corporation, 1791 Deere Ave, Irvine, California 92606, and Solarmer Energy, Inc., El Monte, California 91731

Received: December 8, 2008; Revised Manuscript Received: March 10, 2009

With the aim of revealing the role of additives in polymer solar cells, different amounts of 1,8-octanedithiol (OT) were added to the poly(3-hexylthiophene) (P3HT) and [6,6]-phenyl C61-butyric acid methyl ester (PCBM) blend system in order to observe the transition between systems with and without additive. We found that highly efficient P3HT:PCBM networks can be formed in the very early stage of the spin-coating process when a small amount of additive was added. The carrier mobilities of this fast-grown network were found to be comparable with those processed with solvent annealing. As a result, short circuit current density (J_{sc}) as high as $\sim 9 \text{ mA cm}^{-2}$ can be obtained and the fill factor (FF) can reach $\sim 62\%$. The power conversion efficiency (PCE), however, is limited by the low open circuit voltage (V_{oc}) of the devices processed with OT. According to the grazing incidence X-ray diffraction data, a much shorter interlayer spacing ($d_{(100)} \sim 15.6\text{--}15.7 \text{ \AA}$) compared with those processed with different methods is observed in the polymer blends processed with OT, which is likely the reason for the low V_{oc} .

Introduction

Polymer solar cells based on poly(3-hexylthiophene) (P3HT) and [6,6]-phenyl C61-butyric acid methyl ester (PCBM)^{1–10} have attracted a lot of interest due to the self-assembling property of P3HT, which results in high crystallinity and therefore high carrier mobility.^{11–13} Thermal annealing^{14,15} and solvent annealing^{9,10} are two of the major methods used so far to improve the efficiency of solar cells based on P3HT:PCBM. Power conversion efficiency of 5.5% for polymer solar cell based on poly[2,6-(4,4-bis(2-ethylhexyl)-4H-cyclopenta[2,1-*b*;3,4-*b'*]dithiophene)-*alt*-4,7-(2,1,3-benzothiadiazole)] (PCP-DTBT) has been achieved by incorporating a small volume ratio of alkanedithiols into polymer solutions.¹⁶ Even though the exact mechanism behind the observed increase in efficiency is still not very clear yet, this has attracted a lot of interest in mixed-solvent^{17,18} processing, which gives more flexibility in solution-processed polymer solar cells toward optimized performance. Recently, Yao et al.¹⁹ had reported that addition of 1,8-octanedithiol (OT) and other additives to the P3HT:PCBM system (with dichlorobenzene, DCB, as solvent) can significantly improve the device performance of P3HT:PCBM solar cells under high spin-coating rate (2000 rpm). The mechanism was attributed to the low solubility of PCBM in OT compared with that in DCB, which aggregates PCBM and leaves more room for P3HT to undergo the crystallization process.

Even though the improvement in efficiency of P3HT:PCBM solar cells by adding OT has been found to be effective, there is a lack of full understanding of the effect of OT. In this study, we have performed a detailed investigation of the effect of OT

in P3HT:PCBM blends. Several experiments that include current density–voltage (J – V) characteristics, absorption, external quantum efficiency (EQE), photoluminescence (PL), grazing incidence X-ray diffraction (GIXD), atomic force microscopy (AFM), light intensity dependence, and transient absorption (TA) have been done to clarify the influence of OT on the P3HT/PCBM device performance. By comparing the characteristics of devices made by different methods (such as solvent annealing and/or thermal annealing), an insight of the network formation during the spin-coating process (with OT as additive) is studied.

Experimental Methods

P3HT (purchased from Rieke Metals and used as received) and PCBM (purchased from Nano-C and used as received) with 1:1 weight ratio (20 mg/mL for each) are first dissolved in chlorobenzene (CB; purchased from Sigma Aldrich and used as received) and well mixed (hereafter referred to as base solution). Different amounts of OT (1, 2, 5, 7.5, 15, 20 μL ; purchased from Sigma Aldrich and used as received) are then added to 250 μL base solutions. For example, 5 μL OT solution is made by adding 5 μL of OT into a 250 μL base solution. The solutions with OT are then stirred for more than 10 min. No difference in device performance is observed with different stirring time after adding OT. It has been found that P3HT self-crystallizes, even during the spin-coating process when higher boiling point (T_b) solvent such as dichlorobenzene (DCB, $T_b = 180 \text{ }^\circ\text{C}$) is used.¹⁰ To limit the crystallization during the spin-coating process, CB ($T_b = 131 \text{ }^\circ\text{C}$) was purposely chosen as the major solvent to study the influence of OT on device performance. A PEDOT:PSS (Baytron P VP Al 4083) layer was pre-coated onto the ITO substrate before spin-casting the solutions, where PEDOT:PSS is poly(ethylenedioxythiophene): polystyrene sulfonate. All the solutions were then spin-coated at 3000 rpm for 70 s to make polymer films with different

* Corresponding author. E-mail: yangy@ucla.edu.

[†] University of California—Los Angeles.

[‡] Inha University.

[§] Newport Corp.

^{||} Solarmer Energy, Inc.

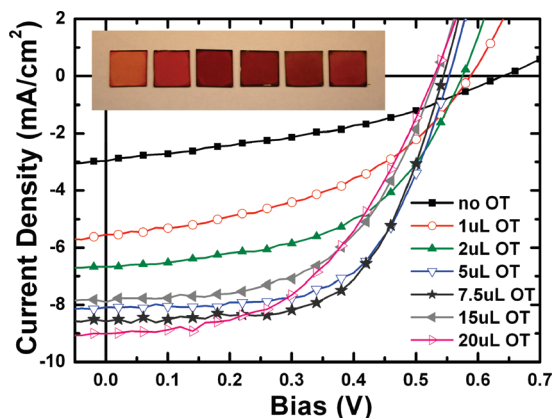


Figure 1. Current density–voltage (J – V) characteristics of devices made with different amounts of OT. Better device performance can be clearly seen upon increasing amount of OT when OT is less than 7.5 μL . Inset: spin-coated polymer films on ITO-covered glass with 0, 1, 5, 7.5, 15, or 20 μL of OT (per 250 μL of base solution) from left to right, respectively.

amounts of OT. A bilayer cathode consisting of a calcium layer (20 nm) and subsequently an aluminum layer (100 nm) was deposited by thermal evaporation under vacuum (1×10^{-6} Torr). The active area for all the devices discussed here was $\sim 12 \text{ mm}^2$. The polymer films spin-coated on ITO-covered glass are shown in the inset of Figure 1. Note that the colors of all the films do not change with time after spin coating. The polymer films shown in the inset of Figure 1 are with 0, 1, 5, 7.5, 15, 20 μL of OT (per 250 μL of base solution) from left to right, respectively. For the film without any additive, it shows light orange color. After 1 μL OT was added to the base solution (250 μL), the change in color of the polymer film from orange to red is obvious. When more OT was added to the base solution, e.g., 5 μL of OT, the film became purple, which is very similar to the color of solvent annealed P3HT:PCBM film.^{9,10} Further increasing the amount of OT did not change the color of the film significantly. However, when more than 15 μL of OT is added, the film starts to become foggy due to serious phase separation, and the film color becomes slightly lighter purple. It is interesting that the polymer films with OT additive changed color within 5 s of the spin-coating process, which suggests the solvent evaporated very fast during this time period.

The J – V curves of all the devices are measured using a Keithley 2400 source-measure unit. A calibrated solar simulator (Oriel) with 100 mW/cm^2 power density was used as the light source. Neutral density filters are used to change the light intensity for the intensity-dependence study. For EQE measurement, a xenon lamp (Oriel, model 66150, 75 W) was used as light source, and a chopper and lock-in amplifier were used for phase sensitive detection. The wavelength was controlled using a monochromator. To ensure an accurate counting of incident photons, a calibrated Si photodiode was used as a reference device.

The absorption spectra were taken using a Varian Cary 50 ultraviolet–visible spectrophotometer. AFM images were obtained using a Digital Instruments multimode scanning probe microscope.

Results and Discussion

Device Characterization. Figure 1 shows the current density–voltage (J – V) curves of the devices with different amounts of OT as additive. The device without any additive represents poor photovoltaic characteristic due to the fragmental

interpenetrating network formed during such high spin rate (3000 rpm) with low boiling point solvent, CB, which significantly reduces the time available for P3HT to undergo crystallization.¹⁰ However, when a tiny amount of OT (1 μL OT/250 μL solution) is added, the short-circuit current density (J_{sc}) almost doubled. Similar phenomenon has been observed recently by using DCB as the major solvent.¹⁹ Upon further increasing the amount of OT, the J_{sc} kept increasing, except for a small drop for 15 μL OT device. On the other hand, the open-circuit voltage dropped monotonically with increasing amount of OT.

To study the influence of OT on P3HT:PCBM solar cell devices, more than 20 devices have been made and the averaged value of each factor [V_{oc} , J_{sc} , fill factor (FF), and power conversion efficiency (PCE)] with its error bars are shown in Figure 2. Devices made with solutions made at different times show high reproducibility. As shown in Figure 2a, the average value of V_{oc} drops from 0.65 V (0 μL of OT) to 0.53 V (20 μL of OT) with increasing amount of OT. Most of the V_{oc} drop is observed when a small amount of OT (<5 μL) is added. The much wider error bar of the device without OT is due to the sensitivity of V_{oc} to the degree of P3HT crystallinity,¹⁰ which varies with the solvent evaporation rate. Fluctuation of environmental conditions during the spin-coating process, such as temperature and/or solvent vapor pressure inside the glovebox, should change the solvent evaporation rate during the spin-coating process. This is more obvious when lower boiling point solvent is used. However, devices with OT perform more consistently (smaller error bar), and for the devices with 5 μL of OT the V_{oc} is almost a fixed value for devices made at different times. While V_{oc} dropped with increasing amount of OT, J_{sc} increases significantly when more OT is added and it saturates for 7.5 μL of OT additive, as shown in Figure 2b. The increase in J_{sc} is very similar to that observed during the solvent-annealing process.¹⁰ Interestingly, different from the solvent-annealing effect, FF increases significantly with a small amount of OT (<5 μL) but decreases with a further increase in the amount of OT (Figure 2c). We also observed a monotonic decrease in series resistance with increasing amount of OT (not shown here). Thus, the decrease in FF with higher amount of OT (>7.5 μL) is attributed to the decrease in shunt resistance, which is likely due to the serious phase separation when more and more OT is added. As a result, the PCE initially increases until a peak value due to the increase in both J_{sc} and FF and then decreases as a result of the decrease in both V_{oc} and FF. The optimized concentration is around 7.5 μL of OT added to 250 μL of base solution. Note that the highest PCE obtained by this concentration is $\sim 3.1\%$, which is slightly lower than the performance of solvent-annealed ($\sim 3.5\%$) device without thermal annealing.¹⁰ It is surprising that adding a small amount of OT can improve the device performance significantly during the fast spin-coating process. All the device parameters are summarized in Table 1.

Absorption Spectra, Photoluminescence, and External Quantum Efficiency. Absorption spectrum, photoluminescence (PL), and external quantum efficiency (EQE) are used to unveil which of the fundamental photovoltaic conversion processes, viz., exciton generation, dissociation, and carrier collection, is responsible for the improved performance of devices with small amounts of OT additive. Figure 3a represents the absorption spectrum change with different amounts of OT additive. The thickness of all the films is listed in Table 2. Previous study has shown that the red-shift of the main absorption peak with the three vibronic shoulders (at ~ 515 , 550, and 610 nm) is an expression of strong interchain–interlayer interactions or high

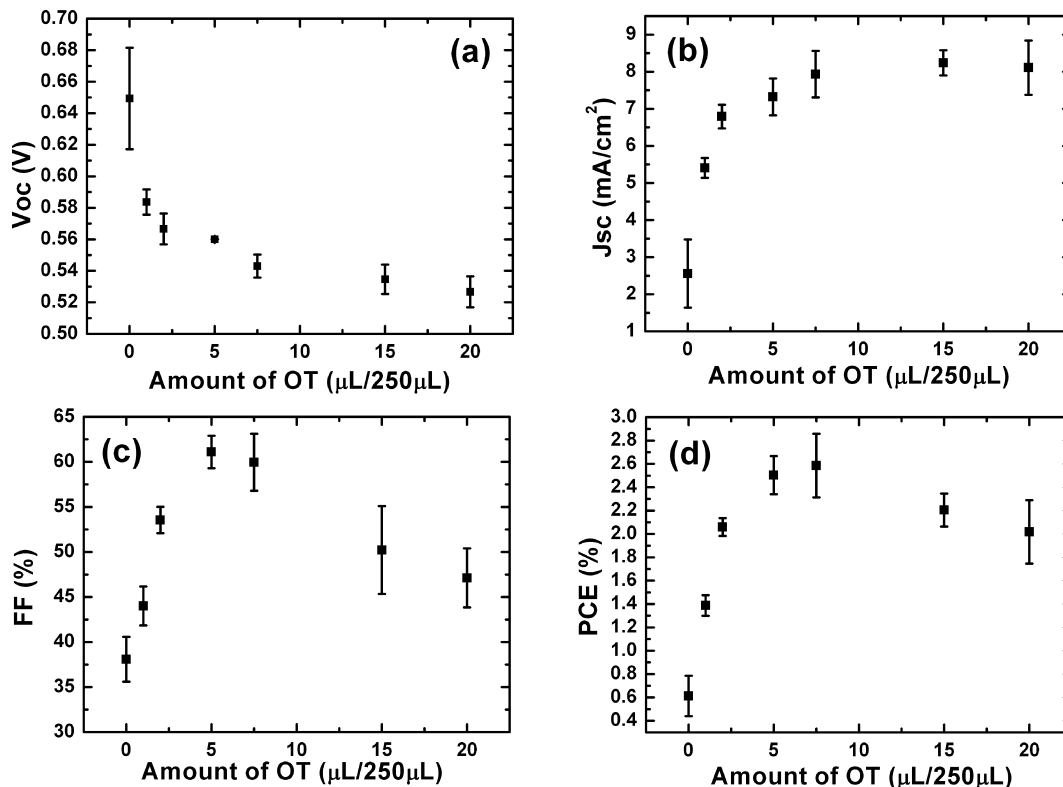


Figure 2. V_{oc} (a), J_{sc} (b), FF (c), and PCE (d) change with different amounts of OT.

TABLE 1: List of Parameters of Devices Made with Different Amount of OT^a

microliters of OT added to 250 μL of base solution ^b	V_{oc} (V)	J_{sc} (mA/cm^2)	FF	PCE (%)
0	0.65	2.6	0.38	0.6
1	0.58	5.4	0.44	1.4
2	0.57	6.8	0.54	2.1
5	0.56	7.3	0.61	2.5
7.5	0.54	7.9	0.60	2.6
15	0.53	8.2	0.50	2.2
20	0.53	8.1	0.47	2.0

^a More than 20 devices were made, and the averaged values are shown. ^b Base solution is composed of 2% P3HT:PCBM with 1:1 weight ratio in CB.

crystallinity of P3HT.^{10,20} The change in absorption spectrum from 0 to 5 μL of OT follows the trend of relatively amorphous film for no OT to crystalline P3HT features when OT is added. When more than 5 μL of OT is added, the peak positions no longer change but only a drop in absorbance is observed. To confirm whether the crystallization of P3HT occurs in solution or during the spin-coating, we measured the absorption of P3HT:PCBM solutions with (5, 30, or 40 μL of OT added to 250 μL) and without OT. The absorption of these solutions was taken by sandwiching the polymer solution between two glass slides so that the real behavior of polymer molecules in the solution can be imitated. There is no shift of peak observed between these solutions, even for solution with 40 μL of OT additive, suggesting that the crystallization of P3HT happens during the solvent drying (or spin coating) process and not in the solution state. The effect of additive on different polymers in solution has been reported recently.^{21,22} However, we did not observe a similar effect in the P3HT:PCBM system with OT as additive. We believe that the addition of OT in P3HT:PCBM system is more related to the mixed-solvent effect, instead of changing

the intrinsic property such as crystallization of P3HT in solution within this OT concentration range.

Mixed-solvent-assisted crystallization of semicrystalline polymers has been reported by Wong et al.²³ In their work, water/methanol was chosen as a mixed solvent and solvent-induced crystallization of a semicrystalline polymer, poly(vinyl alcohol), was observed. It is also observed that significant crystallization happens during the fast solvent evaporation process. To confirm if the phase separation as well as the crystallization of P3HT are completed at the time the films undergo color change (those with OT) during spin coating process, we manually stopped the spin coating after 5 s (around the time the films just change color). It is surprising that the devices perform the same as those spin-coated for 70 s, suggesting that the main network has been formed within 5 s during the spin-coating process. Our previous work¹⁹ shows that the addition of OT helps in the crystallization of P3HT (without PCBM), as observed by the absorption spectrum. Aggregation of PCBM was also observed in different polymer/PCBM systems when OT is added.²⁴ The aggregation of PCBM is required to form a continuous pathway for electrons to transport to the electrode, and on the other hand, it also provides more space for P3HT to undergo crystallization.^{10,19} It is likely that both the aggregation of PCBM and solvent-induced P3HT crystallization contribute to the fast-grown fine interpenetrating network during the spin-coating process.

Photoluminescence was done by exciting the polymer film with 517 nm wavelength light. Absorption of each corresponding polymer film at this wavelength is used to normalize the obtained PL intensity. As shown in Figure 3b, the PL intensity increases with increasing amount of OT. It is known that the PL intensity of P3HT increases when the conjugation length increases²⁵ or when the domain size of P3HT increases.²⁶ While PCBM is known to quench the PL of P3HT effectively,⁸ the increase in PL intensity suggests the interface area between P3HT and PCBM is decreasing. The phase separation seems to

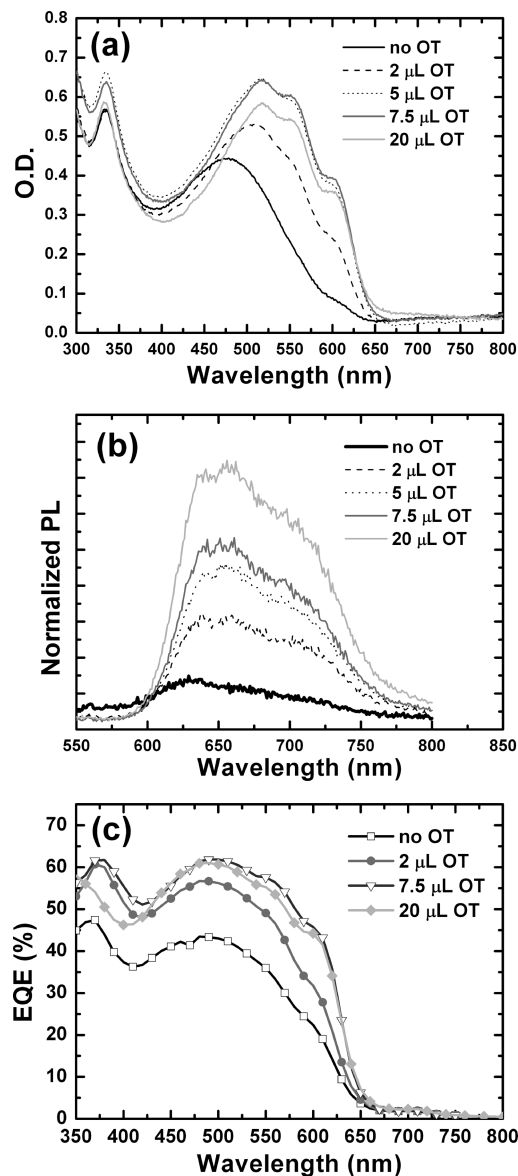


Figure 3. Absorption (a), PL (b), and EQE (c) change with different amounts of OT.

be more serious when more OT is added, which is likely due to the different solubility of P3HT and PCBM in OT^{16,24} or the different solubility of PCBM in OT and CB.¹⁹

After excitons dissociate at the P3HT/PCBM interface, efficient carrier collection is required for a high-efficiency solar cell. We used EQE to examine the carrier transport in the interpenetrating network formed during the spin-coating process. Good carrier transporting pathways are formed during the fast spin-coating process, which gave a device with $\sim 62\%$ EQE at optimized condition (7.5 μL of OT/250 μL of solution), as shown in Figure 3c. This value is very close to the value obtained from solvent-annealed devices reported before,¹⁰ consistent with the fact that the J_{sc} values obtained from these two methods are very close. Note that the shape of the EQE curve obtained from P3HT:PCBM with OT additive is very different from that of the solvent-annealed P3HT:PCBM device. The red-shift of PCBM peak is likely due to the different optical field distribution inside the film caused by different film thickness and/or different distribution of P3HT and PCBM.²⁷

Grazing Incidence X-ray Diffraction and Mobility Measurement. It has been known that the color variations in either solid or liquid state of π -conjugated organic materials are mainly

related to changes in crystallinity. π -Conjugated ordering of P3HT is one of the prominent examples.²⁸ Synchrotron-based grazing incidence X-ray diffraction (GIXD) was performed for the as-spun P3HT:PCBM films. Figure 4a represents 2-D GIXD patterns of the as-spun P3HT:PCBM films with different loading of OT. In all these polymer blend films, the orientation of P3HT maintains edge-on structure with respect to the substrate, irrespective of the OT content, i.e., the hexyl side chains and backbone of P3HT are oriented perpendicular and parallel to the surface, respectively.² However, the crystallinity of P3HT in the films significantly increases with the presence of OT and tends to keep steady above 5 μL OT, as indicated in 1-D out-of-plane X-ray profiles normalized by film thicknesses (see Figure 4b). In particular, the addition of OT remarkably changes the average interlayer spacing, $d_{(100)}$, in P3HT crystals from 16.5 \AA (for 0 μL OT) to 15.6–15.7 \AA (inset of Figure 4b). Such short interlayer spacing ($d_{(100)} \sim 15.6\text{--}15.7 \text{\AA}$) has not been observed in P3HT and/or P3HT:PCBM films with different processing methods such as as-spun ($\sim 16.5 \text{\AA}$, inset of Figure 4b), thermally annealed ($\sim 16.4 \text{\AA}$ ¹⁵), and solvent-annealed ($\sim 16.1 \text{\AA}$ ¹⁰). This implies that the interaction between P3HT is stronger with the presence of OT; i.e., the P3HT molecules are better “packed”. In our previous work, the decrease of V_{oc} in solvent-annealed P3HT:PCBM devices is attributed to the stronger interchain–interlayer interactions due to the better crystallization of P3HT.¹⁰ The stronger interactions likely reduce the effective “band gap” relative to the HOMO (of P3HT) – LUMO (of PCBM) difference.²⁹ Note that the V_{oc} of devices with OT is much lower than that of thermally annealed¹⁵ or solvent-annealed devices,¹⁰ as shown in Figure 2a. Even though there is no evidence of direct relation between the strength of polymer–polymer interactions (or the interlayer spacing) and V_{oc} reported so far, here we observe a lower V_{oc} , corresponding to the smaller interlayer spacing. On the other hand, the size distribution of P3HT crystals is broader with increasing amount of OT, as shown in Figure 4c.

Segmental aggregation caused by addition of a poor solvent has been reported in poly[2-methoxy-5-(2'-ethylhexyloxy)-1,4-phenylenevinylene] (MEH-PPV)³⁰ solution recently. The polymer chains tend to aggregate so that the interaction between polymer and the poor solvent molecules can be minimized. The better crystallization of P3HT and broader crystal size distribution with higher OT concentration can thus be explained as follows. During the spin-coating process, the major solvent (CB) evaporates much faster than the poor solvent (OT), which results in a sudden increase of the volume ratio of the poor solvent to the major solvent. To lower the internal energy, the polymer molecules tend to aggregate when the poor solvent volume ratio reaches some critical point. With more OT, the time required to reach this critical point is shorter during the spin-coating process. Besides, the higher ratio of poor solvent (more amount of OT) provides a stronger driving force for polymer aggregation. As a result, the polymer molecules aggregate with larger average domain size due to the stronger driving force and present broader size distribution due to the shorter aggregation time.

Highly ordered π -conjugated pathways are known to benefit the carrier mobility in the polymer film. The carrier mobilities in the P3HT:PCBM devices with and without OT additive were studied here by using the space charge limited current (SCLC)³¹ method reported before. Experimental parameters are the same as in our previous work, except that the V_{bi} used for electron only devices is 0.1 V while that for hole only devices is -0.5 V. The calculated electron and hole mobility are shown in Table 2 with corresponding film thickness. For easier comparison, the

TABLE 2: List of Thickness and Mobility of Devices Made with Different Amounts of OT and Mobility of Devices Reported Before

microliters of OT added to 250 μL base solution ^a	thickness (\AA)	hole mobility ($\text{cm}^2/\text{V s}$)	electron mobility ($\text{cm}^2/\text{V s}$)	fast grown ^b		solvent annealed ^c	
				hole mobility ($\text{cm}^2/\text{V s}$)	electron mobility ($\text{cm}^2/\text{V s}$)	hole mobility ($\text{cm}^2/\text{V s}$)	electron mobility ($\text{cm}^2/\text{V s}$)
0	1650	2.6×10^{-6}	5.7×10^{-4}	1.9×10^{-5}	6.5×10^{-4}	1.7×10^{-3}	2.6×10^{-3}
1	1870	6.2×10^{-5}	3.2×10^{-3}				
2	1900						
5	2150						
7.5	2070	9.4×10^{-4}	2.8×10^{-3}				
15	1980						
20	1980	5.2×10^{-4}	6.1×10^{-3}				

^a Base solution is composed of 2% P3HT:PCBM with 1:1 weight ratio in CB. ^b Fast grown devices are made by spin-coating the P3HT:PCBM film until the film is dried. ^c See ref 31 for details.

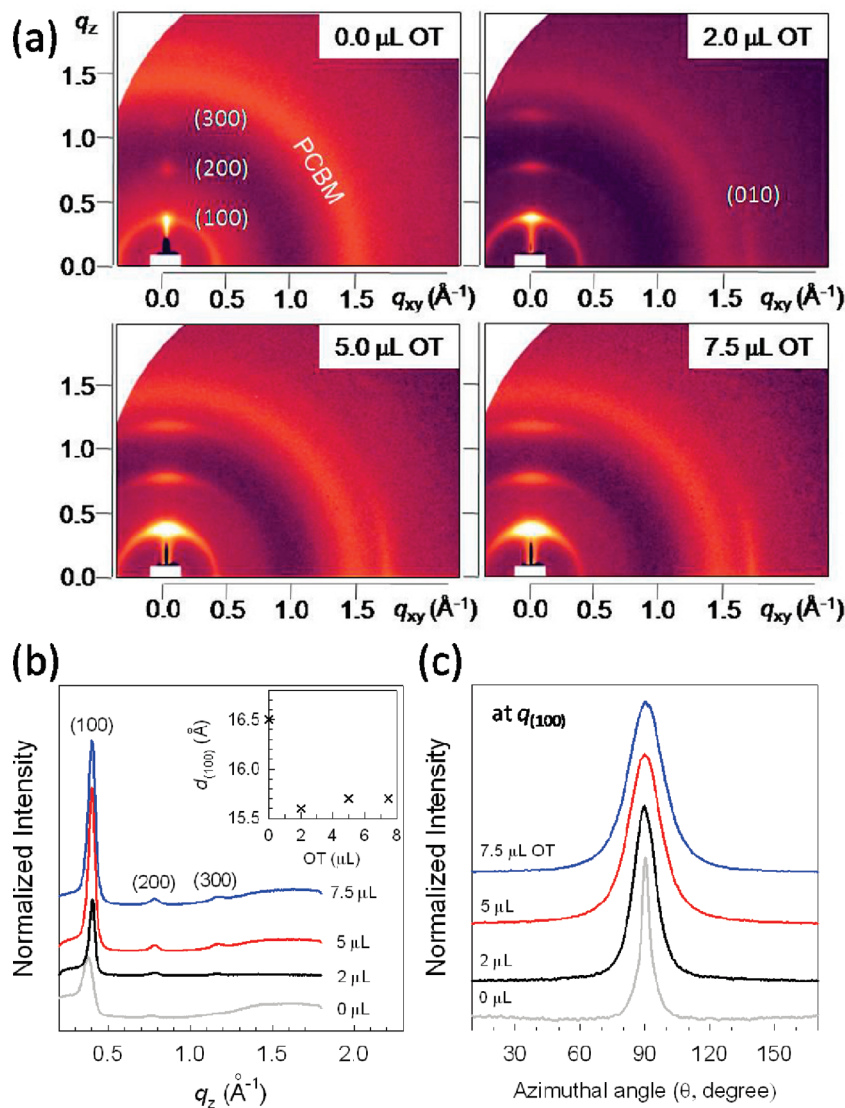


Figure 4. (a) 2D GIXD patterns of films with different amounts of OT. (b) 1D out-of-plane X-ray and (c) azimuthal scan (at $q^{(100)}$) profiles extracted from part a. Inset of b: calculated interlayer spacing in (100) direction with different amounts of OT.

electron and hole mobilities for P3HT:PCBM devices with and without solvent-annealing reported in our previous work³¹ are also shown in Table 2. The electron mobility in the P3HT:PCBM device without OT is very close to the reported value for P3HT:PCBM devices without solvent annealing. However, the hole mobility of P3HT:PCBM device without solvent annealing (DCB as solvent) is 1 order of magnitude higher than that of device without OT (CB as solvent). This suggests that

the higher solvent evaporation rate of the low T_b solvent causes poor hole mobility (due to less crystallinity), as expected. While more and more OT is added, the electron mobility only increases by 1 order of magnitude from the one without OT and finally reaches the value very close to that of the solvent-annealed device. Hole mobility, on the other hand, increases 2 orders of magnitude for devices with 7.5 μL of OT in comparison to devices without OT. The best device performance (7.5 μL OT)

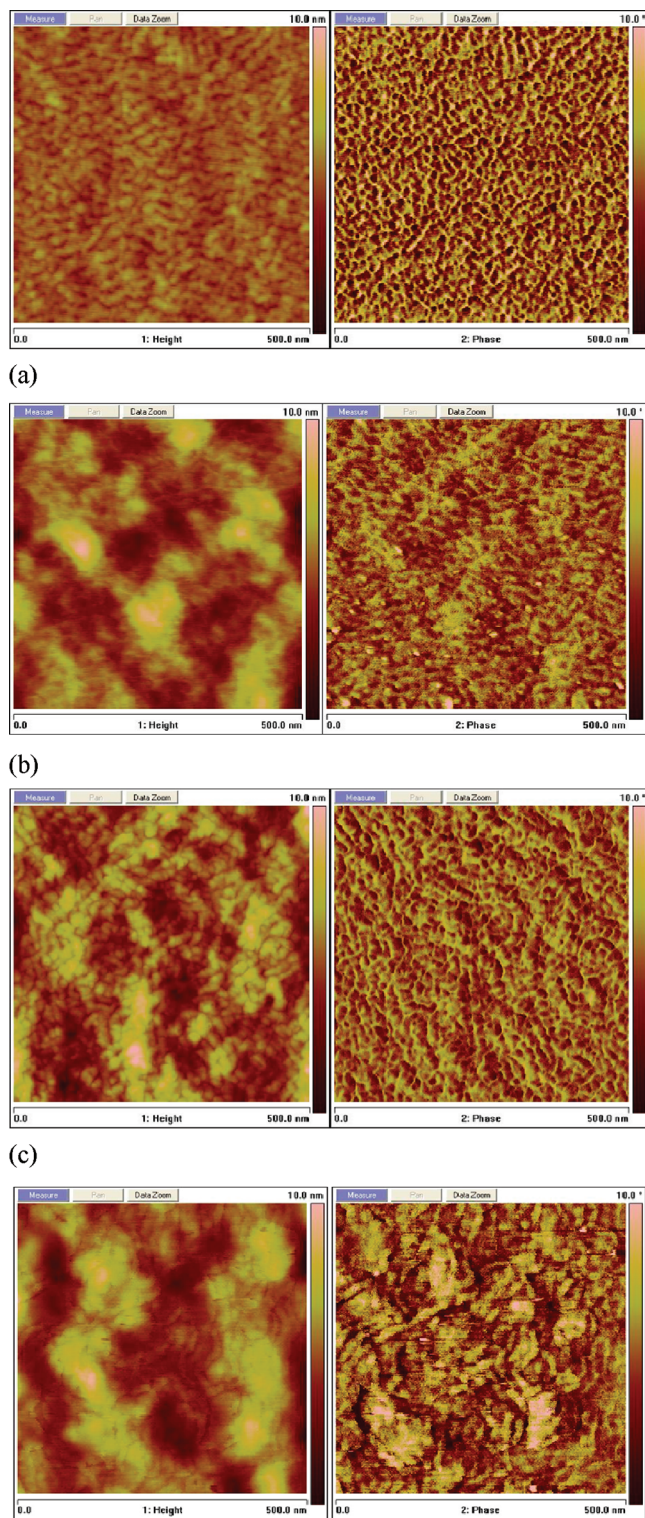


Figure 5. Tapping mode AFM images of films with different amounts of OT in 500 nm × 500 nm. Left: topography. Right: phase images. (a) 0 μL , (b) 7.5 μL , (c) 20 μL , and (d) 40 μL of OT. The scale bars are 10.0 nm in the height images and 10.0° in the phase images.

is obtained when the electron ($2.8 \times 10^{-3} \text{ cm}^2 \text{ V}^{-1} \text{ s}^{-1}$) and hole ($9.4 \times 10^{-4} \text{ cm}^2 \text{ V}^{-1} \text{ s}^{-1}$) mobilities are more comparable.

Morphology Study. From atomic force microscopy (AFM) images (Figure 5), the growth of polymer domains is clearly seen. Parts a, b, c, and d of Figure 5 show the height (left) and phase (right) images of polymer films with 0, 7.5, 20, and 40 μL of OT, respectively. The roughness values obtained are 0.52

nm (0 μL of OT), 1.04 nm (7.5 μL of OT), 1.37 nm (20 μL of OT), and 1.43 nm (40 μL of OT), showing an increasing trend with increasing amount of OT. The domain sizes estimated by cross-section profiles are ~ 10 , 15, 15–25, and 15–25 nm, correspondingly, consistent with the higher crystallization observed with increasing amount of OT. With the fact that the exciton diffusion length in polymer systems is ~ 5 –10 nm,^{32–34} the smaller domain sizes compared with those formed by different processing methods¹⁰ should be the reason for the efficient exciton dissociation as well as carrier collection, which contribute to high J_{sc} . Note that the domain sizes have a wider distribution for 20 and 40 μL OT polymer films, as observed from the phase image (Figure 5c,d, right). This is also consistent with the GIXD results, which show wider domain size distribution with increasing amount of OT. Finely dispersed structure is observed when there is no OT added (Figure 5a). Thin fibrillar structure starts to appear when 7.5 μL of OT is added (Figure 5b) and the P3HT domain grows even bigger when 20 and 40 μL of OT are added (Figure 5c,d, respectively). The high J_{sc} of 7.5 μL OT device as well as its high EQE proved that the charge transport is efficient within these tiny fibrillous structure. The growth of P3HT domains is also consistent with the PL spectra, which show that the interface area of P3HT/PCBM is decreasing (higher PL intensity when more and more OT is added; Figure 3b). The decreased interface area does not result in the decrease of J_{sc} , showing that the P3HT domain size is still beneficial for exciton dissociation. We also made devices by using solutions with 30 and 40 μL of OT. Interestingly, the J_{sc} becomes even higher ($\sim 10 \text{ mA/cm}^2$) than that of 20 μL OT devices ($\sim 9 \text{ mA/cm}^2$), even though serious phase separation is observed in these films. This suggests that the carrier dissociation is still efficient within these devices. The device performances, however, are limited by the low fill factors caused by the serious phase separation as well as the low V_{oc} .

Light Intensity Dependence and Transient Absorption Study. To have an insight into the photoconversion process in these devices, light intensity dependence was studied, and the results are shown in Figure 6. For all devices, V_{oc} shows linear dependence with logarithmic light intensity with a slope around 0.06 ($\sim kT/q$), as shown in Figure 6a. Similar behavior has been reported in different polymer blend systems.^{35,36} Light intensity dependence of J_{sc} is shown in Figure 6b in a double-logarithmic diagram. The slopes of the curves for 0, 1, 7.5, and 20 μL of OT are 0.8, 0.97, 1, and 0.99, respectively. Previous studies³⁵ have shown that a slope close to 1 indicates that the carrier loss is dominated by monomolecular (or geminate) recombination, while the deviation from 1 results from bimolecular (or nongeminate) recombination.³⁷ The change in slope, as well as the sudden increase in J_{sc} value, suggests that the bimolecular recombination is significantly reduced when 1 μL of OT is added, possibly due to the more evolved percolation pathway. The fill factor change with light intensity is shown in Figure 6c. For the device without OT, FF is less dependent on light intensity when light intensity is higher than 20 mW/cm^2 . However, when OT is added, the FF increases significantly with decreasing light intensity. It is known that FF depends on shunt resistance and serial resistance in a complex way. According to the J – V curve, the increase in FF with decreasing light intensity is attributed to the increase in shunt resistance. PCE as a combined result of V_{oc} , J_{sc} , and FF is shown in Figure 6d for reference.

Transient absorption (TA) of fast- and slow-grown films and films with 1 and 7.5 μL of OT as additive was measured with 35 fs time resolution. The samples were excited with 400 nm

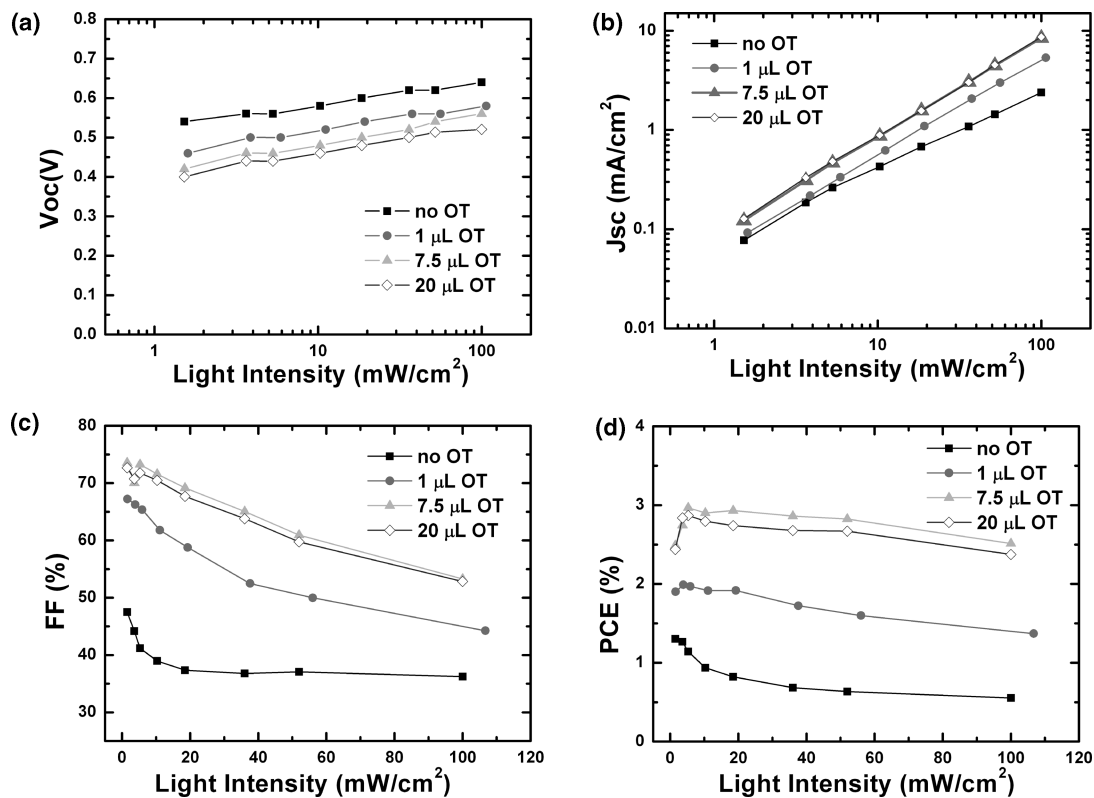


Figure 6. Light intensity dependence of (a) V_{oc} , (b) J_{sc} , (c) FF, and (d) PCE for devices with different amounts of OT.

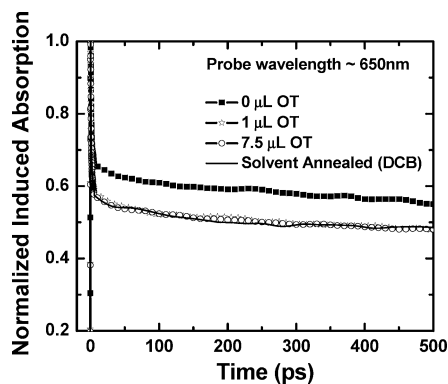


Figure 7. Comparison of induced absorption decay measured at probe wavelength of 650 nm for P3HT:PCBM blend films formed under different conditions.

and probed with white light. The photoinduced absorption (PIA) corresponding to probe wavelength of 650 nm and longer is dominated by the absorption due to the free carriers that are generated after exciton dissociation at P3HT/PCBM interface. Figure 7 shows the decay of the normalized PIA at 650 nm for P3HT:PCBM films grown under different conditions. The induced absorption consists of initial fast decay followed by a slow decay component. The normalized induced absorption for fast-grown films is slightly higher than that of solvent-annealed films and films formed from CB with OT additive. Higher induced absorption from fast-grown films implies that more carriers are generated as a result of exciton dissociation, which is consistent with the stronger PL quenching observed in fast-grown films over other P3HT:PCBM blend films. On the other hand, the induced absorption for films from CB solution with small amount OT additive (~ 1 or $7.5 \mu\text{L}$) is comparable to that of slow-grown films. This shows that addition of small amounts of OT additive leads to pronounced phase segregation of P3HT

and PCBM domains, thereby reducing the donor/acceptor interface area.

In spite of the greater generation of free carriers in fast-grown films, the observed J_{sc} is much smaller as compared to other films. This is because of the increased nongeminate recombination observed in fast-grown films, as evidenced in the light intensity dependence of J_{sc} . On the time scale of our PIA measurements (< 1 ns), we do not observe any significant decrease in induced absorption due to nongeminate recombination, possibly because the time scale of nongeminate recombination is on the order of a few tens of nanoseconds.

Conclusions

The effect of OT on the performance of P3HT:PCBM solar cells has been studied by different experimental measurements. A fast-grown interpenetrating network is formed during the fast spin-coating process when OT is added to the P3HT:PCBM solution. The presence of the poor solvent (OT) for P3HT and PCBM forces both P3HT and PCBM to aggregate when the major solvent (CB) starts to evaporate out during the spin-coating process. The comparable J_{sc} values obtained with thinner film (less absorption) compared with solvent annealed devices suggest that the exciton dissociation and carrier collection are rather efficient in the devices made with OT. Clear domain growth can be observed through GIXD and AFM when more and more OT is added. The interlayer spacing of P3HT in the films processed with OT is much shorter compared with those processed with other methods reported so far. The poor solubility of P3HT in OT is likely the driving force of this shorter interlayer spacing. More works on the additive effect of different polymer systems are needed for better manipulation of poor solvents in improving the morphology as well as device performances in polymer solar cells.

Acknowledgment. This work is financially supported by Solarmer Energy Inc. (Grant No. 20061880). R.Z. thanks Mr. John Carter for assistance with TA measurements.

References and Notes

- (1) Padinger, F.; Rittberger, R. S.; Sariciftci, N. S. *Adv. Funct. Mater.* **2003**, *13*, 85.
- (2) Erb, T.; Zhokhavets, U.; Gobsch, G.; Raleva, S.; Stuhn, B.; Schilinsky, P.; Waldauf, C.; Brabec, C. J. *Adv. Funct. Mater.* **2005**, *15*, 1193.
- (3) Schilinsky, P.; Asawapirom, U.; Scherf, U.; Biele, M.; Brabec, C. J. *Chem. Mater.* **2005**, *17*, 2175.
- (4) Kim, Y.; Cook, S.; Tuladhar, S. M.; Choulis, S. A.; Nelson, J.; Durrant, J. R.; Bradley, D. D. C.; Giles, M.; McCulloch, I.; Ha, C. S.; Ree, M. *Nat. Mater.* **2006**, *5*, 197.
- (5) Mihailetchi, V. D.; Xie, H. X.; de Boer, B.; Koster, L. J. A.; Blom, P. W. M. *Adv. Funct. Mater.* **2006**, *16*, 699.
- (6) Chirvase, D.; Chiguvare, Z.; Knipper, M.; Parisi, J.; Dyakonov, V.; Hummelen, J. C. *J. Appl. Phys.* **2003**, *93*, 3376.
- (7) Al-Ibrahim, M.; Ambacher, O.; Sensfuss, S.; Gobsch, G. *Appl. Phys. Lett.* **2005**, *86*, 3.
- (8) Kim, Y.; Choulis, S. A.; Nelson, J.; Bradley, D. D. C.; Cook, S.; Durrant, J. R. *J. Mater. Sci.* **2005**, *40*, 1371.
- (9) Li, G.; Shrotriya, V.; Huang, J.; Yao, Y.; Tommoriarty; Emery, K.; Yang, Y. *Nat. Mater.* **2005**, *4*, 864.
- (10) Li, G.; Yao, Y.; Yang, H.; Shrotriya, V.; Yang, G.; Yang, Y. *Adv. Funct. Mater.* **2007**, *17*, 1636.
- (11) Sirringhaus, H.; Brown, P. J.; Friend, R. H.; Nielsen, M. M.; Bechgaard, K.; Langeveld-Voss, B. M. W.; Spiering, A. J. H.; Janssen, R. A. J.; Meijer, E. W.; Herwig, P.; de Leeuw, D. M. *Nature (London)* **1999**, *401*, 685.
- (12) Kim, D. H.; Park, Y. D.; Jang, Y. S.; Yang, H. C.; Kim, Y. H.; Han, J. I.; Moon, D. G.; Park, S. J.; Chang, T. Y.; Chang, C. W.; Joo, M. K.; Ryu, C. Y.; Cho, K. W. *Adv. Funct. Mater.* **2005**, *15*, 77.
- (13) Mihailetchi, V. D.; Xie, H. X.; de Boer, B.; Popescu, L. M.; Hummelen, J. C.; Blom, P. W. M.; Koster, L. J. A. *Appl. Phys. Lett.* **2006**, *89*, 012107.
- (14) Li, G.; Shrotriya, V.; Yao, Y.; Yang, Y. *J. Appl. Phys.* **2005**, *98*, 043704.
- (15) Ma, W. L.; Yang, C. Y.; Gong, X.; Lee, K.; Heeger, A. J. *Adv. Funct. Mater.* **2005**, *15*, 1617.
- (16) Peet, J.; Kim, J. Y.; Coates, N. E.; Ma, W. L.; Moses, D.; Heeger, A. J.; Bazan, G. C. *Nat. Mater.* **2007**, *6*, 497.
- (17) Jin, S. H.; Naidu, B. V. K.; Jeon, H. S.; Park, S. M.; Park, J. S.; Kim, S. C.; Lee, J. W.; Gal, Y. S. *Sol. Eng. Mater. Sol. Cells* **2007**, *91*, 1187.
- (18) Chen, F. C.; Tseng, H. C.; Ko, C. J. *Appl. Phys. Lett.* **2008**, *92*, 103316.
- (19) Yao, Y.; Hou, J.; Xu, Z.; Li, G.; Yang, Y. *Adv. Funct. Mater.* **2008**, *18*, 1783.
- (20) Sundberg, M.; Inganäs, O.; Stafstrom, S.; Gustafsson, G.; Sjogren, B. *Solid State Commun.* **1989**, *71*, 435.
- (21) Cook, S.; Furube, A.; Katoh, R. *Jpn. J. Appl. Phys.* **2008**, *47*, 1238.
- (22) Peet, J.; Brocker, E.; Xu, Y. H.; Bazan, G. C. *Adv. Mater.* **2008**, *20*, 1882.
- (23) Wong, S. S.; Altinkaya, S. A.; Mallapragada, S. K. *Polymer* **2004**, *45*, 5151.
- (24) Lee, J. K.; Ma, W. L.; Brabec, C. J.; Yuen, J.; Moon, J. S.; Kim, J. Y.; Lee, K.; Bazan, G. C.; Heeger, A. J. *J. Am. Chem. Soc.* **2008**, *130*, 3619.
- (25) Bai, X.; Holdcroft, S. *Macromolecules* **1993**, *26*, 4457.
- (26) Zhokhavets, U.; Erb, T.; Hoppe, H.; Gobsch, G.; Sariciftci, N. S. *Thin Solid Films* **2006**, *496*, 679.
- (27) Sylvester-Hvid, K. O.; Ziegler, T.; Riede, M. K.; Keegan, N.; Niggemann, M.; Gombert, A. *J. Appl. Phys.* **2007**, *102*, 054502.
- (28) Yang, H.; LeFevre, S. W.; Ryu, C. Y.; Bao, Z. N. *Appl. Phys. Lett.* **2007**, *90*, 172116.
- (29) Brabec, C. J.; Cravino, A.; Meissner, D.; Sariciftci, N. S.; Fromherz, T.; Rispen, M. T.; Sanchez, L.; Hummelen, J. C. *Adv. Funct. Mater.* **2001**, *11*, 374.
- (30) Traiphon, R.; Charoenthai, N. *Synth. Met.* **2008**, *158*, 135.
- (31) Shrotriya, V.; Yao, Y.; Li, G.; Yang, Y. *Appl. Phys. Lett.* **2006**, *89*, 063505.
- (32) Halls, J. J. M.; Pichler, K.; Friend, R. H.; Moratti, S. C.; Holmes, A. B. *Appl. Phys. Lett.* **1996**, *68*, 3120.
- (33) Haugeneder, A.; Neges, M.; Kallinger, C.; Spirkl, W.; Lemmer, U.; Feldmann, J.; Scherf, U.; Harth, E.; Gugel, A.; Mullen, K. *Phys. Rev. B* **1999**, *59*, 15346.
- (34) Markov, D. E.; Amsterdam, E.; Blom, P. W. M.; Sieval, A. B.; Hummelen, J. C. *J. Phys. Chem. A* **2005**, *109*, 5266.
- (35) Riedel, I.; Parisi, J.; Dyakonov, V.; Lutsen, L.; Vanderzande, D.; Hummelen, J. C. *Adv. Funct. Mater.* **2004**, *14*, 38.
- (36) Koster, L. J. A.; Mihailetchi, V. D.; Ramaker, R.; Blom, P. W. M. *Appl. Phys. Lett.* **2005**, *86*, 123509.
- (37) Meskers, S. C. J.; van Hal, P. A.; Spiering, A. J. H.; Hummelen, J. C.; van der Meer, A. F. G.; Janssen, R. A. J. *Phys. Rev. B* **2000**, *61*, 9917.

JP810798Z